Neuromuscular-System-Based Tuning of a Haptic Shared Control Interface for UAV Teleoperation

Article *in* IEEE Transactions on Human-Machine Systems · August 2017

DOI: 10.1109/THMS.2016.2616280

5 authors, including:

Jan Smisek
Transcelestial Technologies
27 PUBLICATIONS **805** CITATIONS
SEE PROFILE

Emmanuel Sunil
Netherlands Aerospace Centre
38 PUBLICATIONS **566** CITATIONS
SEE PROFILE

Marinus M. Van Paassen
Delft University of Technology
490 PUBLICATIONS **6,819** CITATIONS
SEE PROFILE

David Abbink
Delft University of Technology
225 PUBLICATIONS **5,328** CITATIONS
SEE PROFILE

Neuromuscular System Based Tuning of a Haptic Shared Control Interface for UAV Teleoperation

J. Smisek[1,2], *Student Member, IEEE*, E. Sunil[1], M. M. van Paassen[1], *Senior Member, IEEE*, D. A. Abbink[3], *Senior Member, IEEE*, and M. Mulder[1]

***Abstract*—Haptic guidance is a promising way to support Unmanned Aerial Vehicle (UAV) operators, but the design of haptic guidance forces is often heuristic. This paper describes the design and experimental validation of a systematic neuromuscular analysis based tuning procedure for haptic guidance, here applied to haptic collision avoidance system for UAV tele-operation. This tuning procedure is hypothesized to reduce operator workload as compared to current heuristic tuning methods. The proposed procedure takes into consideration the estimated mechanical response of the neuromuscular system (NMS) to haptic cues. A 'relax task' setting of the NMS, for which reflexive and muscular activation is minimal, is chosen as the design point for tuning the haptic support, as this setting is expected to yield minimal physical workload. The paper first presents a neuromuscular identification experiment, performed to estimate the 'relax task' admittance of an operator's arm. The averaged admittance of a group of subjects ($n = 10$) was then used for tuning the haptic shared controller, which was subsequently evaluated in its ability to support different operators ($n = 12$) in a simulated unmanned aerial vehicle surveillance task. Results show that our novel tuning procedure indeed reduces operator workload and also improves situation awareness compared to haptic settings that ignore the neuromuscular system. In fact, it is shown that over-tuning, which frequently occurs for these heuristically tuned systems, leads to even lower user acceptance scores than interfaces without any haptic support.**

***Index Terms*—Haptic cues, Human-automation Interaction, Human-Vehicle Interface, Musculoskeletal system**

I. Introduction

In Haptic Shared Control (HSC) systems, a human operator and an automatic controller share control of a dynamical process on a common control interface, that serves as the only input to the controlled system [1]. Such design ensures that the operator is continuously informed about the actions of the automation, allowing him/her to stay involved in the decision making process through intuitive haptic interactions [2]. In doing so, HSC has the potential to support operators while mitigating some of the human-machine interaction issues frequently associated with automated control systems, such as loss of skills and situational awareness [1]–[3].

Implementing the actions of the automatic system as additional guidance forces on the control interface allows the operator to decide how to react to these. The operator can do this in two ways: by consciously generating a force to give way or counteract the guidance forces, but also by intentionally changing the neuromuscular system (NMS) properties of the limb interacting with the control interface. In other words, if the operator agrees with the provided automatic's support, he/she can become compliant and give way to the haptic forces. In contrast, if the operator disagrees, he/she can stiffen up to resist the haptic force, effectively overruling the automation. In this manner, the operator can dynamically interact with the automation during the operation [2].

The advantageous adaptability of the operator's neuromuscular system also makes HSC systems challenging to design. To cause the desired control interface position, thereby providing the correct inputs to the controlled system, the HSC system force needs to be correctly scaled to match the instantaneous 'setting' of the operator's arm NMS (i.e., whether the operator's arm is compliant, stiff or in between). Although it may be feasible to estimate the NMS admittance in real-time [4], adapting the HSC system based on adaptation of the operator might lead to undesirable outcomes. For instance, if the operator, by stiffening-up, aims to regain control authority over the controlled system, the automation could adapt to this change by increasing the force scaling, and effectively over-ruling the operator [5]. Therefore, we explored tuning the HSC system to one fixed scaling, that corresponds to a specific (and beneficial) setting of the NMS system. When the operator matches his/her neuromuscular behavior to this expected stiffness, the haptic forces will then cause correctly scaled inputs to the human-in-the-loop system.

It is common practice to heuristically tune this scaling to the satisfaction of the system designer [6]. However, we aim to improve and formalize the tuning process. In our preliminary studies we presented an identification method to measure relax task admittance on realistic haptic control interfaces [7] and then tested its utility in a UAV collision avoidance system [8].

The aim of the current paper is twofold: First, we provide a complete systematic and experimentally validated tuning method that uses the operator's arm relax task setting as the design stiffness. Second, expanding upon our previous studies [7], [8], this research will provide more insight into the interaction of the operators with the haptic cues by investigating the agreement of operators with the provided haptic support and analyzing how this agreement changes based on specific situation during the flight.

We first introduce a haptic collision avoidance system that relies on an artificial force field and explain the available HSC

This research is supported by the Dutch Technology Foundation STW, which is part of the Netherlands Organization for Scientific Research (NWO), and which is partly funded by the Ministry of Economic Affairs.

[1]Faculty of Aerospace Engineering, Delft University of Technology, Delft, the Netherlands; {j.smisek, e.sunil, m.m.vanpaassen, m.mulder}@tudelft.nl

[2]Telerobotics and Haptics Laboratory, ESTEC, European Space Agency, Noordwijk, the Netherlands

[3]Faculty of Mechanical, Maritime and Materials Engineering, Delft University of Technology, Delft, the Netherlands; d.a.abbink@tudelft.nl

tuning choices based on the attainable settings of the human NMS, in Section II. Motivation for the relax-task setting based tuning is discussed in detail. We then identify the challenges associated with obtaining (relax task) neuromuscular admittance measurement on a spring-centered control interface and present an appropriate experimental identification procedure in Section III. In Section IV, relax task tuning, using the average data from the first experiment, is used in a human-in-the-loop experiment simulating UAV teleoperation, to judge user acceptance of the novel tuning procedure. The paper concludes with a comprehensive discussion of the results and summarizes the main conclusions, in Sections V and VI.

II. Neuromuscular based tuning of Haptic Shared Control

This section introduces a human-centered tuning approach for haptic cues that is based on properties and measurements of the operator's arm NMS. First, the UAV collision avoidance system is introduced. Second, neuromuscular properties relevant to the tuning approach are presented together with the theoretical rationale of the tuning method.

A. UAV collision avoidance system and previous work

An interesting application of HSC in aviation is the use of haptic feedback to improve the safety of Unmanned Aerial Vehicles (UAVs) [9]. Previously presented studies augmented the visual feedback from onboard cameras with haptic guidance moments applied on a control interface to help teleoperators in steering a UAV away from obstacles [10]–[14]. All these studies have indicated that such a system improves the safety of teleoperation, but at the cost of increased workload [14], [15]. Similar issues were also reported from systems implemented in car driving domain [1].

These previous HSC systems were designed heuristically, i.e., the HSC force scaling was found by testing different values in a human-in-the-loop study, until satisfactory performance was achieved. For instance, the primary objective of one of the studies was to improve system safety over pure manual control [16]. To realize this goal, the haptic controller was typically tuned to generate very strong haptic guidance moments. While 'over-tuning' haptic cues improved safety, it also biased control authority towards the automation [15]. Recent research has shown that heuristic tuning can result in disagreements between the human operator and the automation on a the neuromuscular level [17].

The difficulty with heuristic tuning has been attributed to the large adaptation range of the neuromuscular system. It was observed that operators are able to adapt their NMS properties such that performance and overall system stability are satisfactory, regardless of the specific tuning used. However, adaptations to non-optimal settings of the NMS, as is often the case with heuristic tuning methods, causes the haptic cues to be perceived as too strong, resulting in increased user discomfort and workload over time [18].

As a objective for the current study, it was hypothesized that in order to improve user acceptance of HSC systems, it is necessary to tune haptic cues such that workload is reduced, but without sacrificing system safety or human control authority over the automation. The motivation was, building on our preliminary studies [7], [19], to provide a systematic and validated tuning method that would achieve the aforementioned objective, without relying on heuristic tuning.

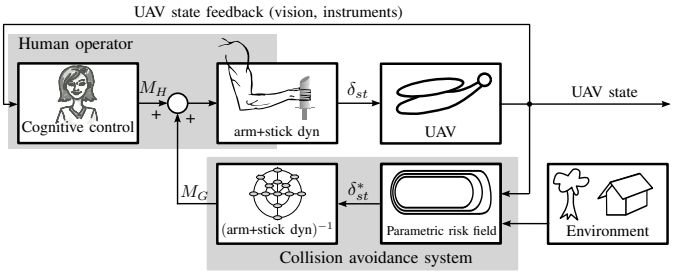

Fig. 1. UAV teleoperation with a haptic *Collision avoidance system*. Based on the UAV state in the environment, the *Parametric risk field* calculates an optimal collision avoidance maneuver, that is scaled by the inverse arm/stick dynamics to a haptic cue on the control side-stick (based on [7]). A method to chose this scaling optimally is the focus of the current paper.

A teleoperated UAV scenario, with addition of the collision avoidance system, is illustrated in Fig. 1. An outer feedback loop to the UAV teleoperator is complemented with an inner haptic feedback loop generated by the collision avoidance system. The operator controls the UAV through the side-stick position δ_{st}. The haptic guidance moment, M_G, and the moment generated by the teleoperator, M_H, act together on the side-stick. The resulting position of the side-stick, δ_{st}, constitutes the sole steering command issued to the UAV.

The collision avoidance system becomes effective only if the UAV flies into a close vicinity of an obstacle. The parametric risk field system scans the environment for obstacles and computes the risk of collision with the corresponding optimal avoidance maneuver [16]. The optimal collision avoidance is achieved with the optimal side-stick position δ^*_{st}. To yield the desired δ^*_{st}, it has to be converted to a properly scaled haptic guidance moment, M_G. The optimal choice of this particular scaling is the focus of the current paper.

B. Properties of the Human Neuromuscular System

Neuromuscular system admittance of the operator arm to external (haptic) forces, i.e., the displacement caused by an external force, is an important parameter for designing HSC systems [20]. The intrinsic NMS properties are formed by the contribution of the skeleton (mainly the inertia) and by the contribution of different muscles (the inertia, stiffness and damping) [21]. However, the NMS is highly adaptive, Fig. 2a, and admittance can be varied over a wide range of values through two physiological mechanisms: fast subconscious spinal reflexes and muscle pair co-contraction [21]. The neuromuscular system uses several sensors located in and near the muscles for its feedback mechanism, such as the muscle spindles and the Golgi Tendon Organs (GTO). The muscle spindles feedback muscle length and muscle velocity and the GTO feed back the force measured in the muscle tendons. The NMS adaptation is achieved by changing the reflex path strength. Stronger muscle spindle feedback produces a position feedback loop that generates a lower admittance (stiffer NMS).

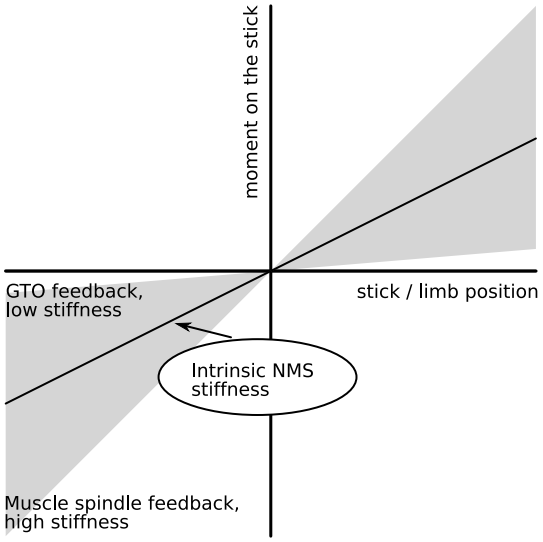

(a) Arm position-force relationship at different NMS settings.

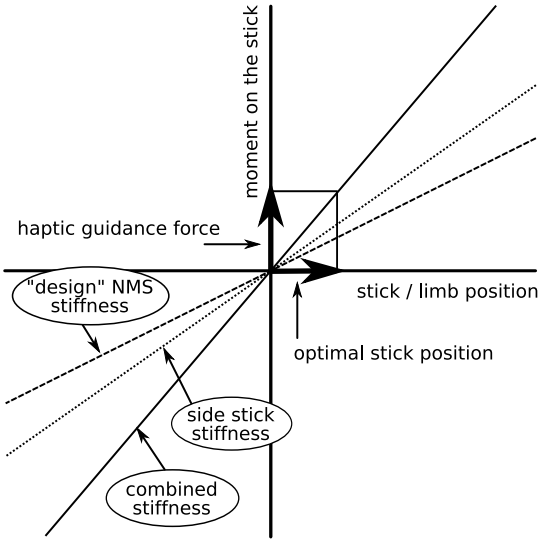

(b) Optimal stick position as result of correctly scaled haptic guidance force.

Fig. 2. Neuromuscular based tuning rationale. Figure (a) illustrates the wide range of arm admittance settings the operator can adopt. The intrinsic stiffness corresponds to relax task situation, when operators do not exert any forces or change their admittance. In (b) the shared control system is tuned to a *design stiffness* which, together with the *side stick* stiffness, forms the *combined stiffness* of the whole system. Figure adapted from [7].

The reverse is also possible, stronger GTO feedback produces a higher admittance (less stiff NMS). Effectively, the stiffness of the neuromuscular system can be raised or lowered through the neural feedback [20]–[22]. To evoke different NMS admittance settings, humans can be instructed to respond to external moments in three distinct ways known in literature as the force, the relax and the position tasks [20], see Table I.

C. Neuromuscular admittance based tuning method

Haptic guidance moments applied on the control interface are transmitted to the human operator via his/her NMS. Therefore it is necessary to include the response of the NMS to haptic cues when tuning the haptic controller [17], [18]. Effectively, this approach uses the inverse of the combined dynamics of the NMS and of the control interface to compute the haptic guidance force, see Fig. 2b. Applying this specific haptic guidance force, assuming the operator keeps the same NMS setting, will result in optimal stick position and consequently in a successful avoidance maneuver. Here, the HSC provides mostly low frequency inputs [16], [19] and so the stick/arm inverse dynamics can be considered as stiffness, yielding a guidance control law:

$$\begin{bmatrix} M_{G_p} \\ M_{G_r} \end{bmatrix} = \underbrace{[\mathbf{K_{NMS}}(\delta_{\mathbf{st}}) + \mathbf{K_{st}}]}_{\text{combined stiffness}} \begin{bmatrix} \delta^*_{st_p} \\ \delta^*_{st_r} \end{bmatrix}, \qquad (1)$$

where $\mathbf{K_{NMS}}$ is the stiffness of the NMS and $\mathbf{K_{st}}$ is the stiffness of the side-stick control interface. The $\mathbf{K_{NMS}}$ and $\mathbf{K_{st}}$ are defined separately along the pitch (p) and roll (r) hand/stick axes. The optimal side-stick input δ^*_{st} in Eq. (1) represents the output of the parametric risk field (described in more detail in Section IV-A3). Note that the tuning law accounts for the dependence of $\mathbf{K_{NMS}}$ on the magnitude and direction of manual control inputs applied on the side-stick, $\delta_{\mathbf{st}}$. To implement the control law described above, a value for $\mathbf{K_{NMS}}$ has to be selected. Three available, NMS inspired, design options are described next.

TABLE I
DESCRIPTION OF THE THREE NEUROMUSCULAR TASK INSTRUCTIONS.

Task	Admittance	Description
Force Task (FT)	High	Yield to haptic moments and the motion of control interface
Relax Task (RT)	Medium	Do not react to haptic moments and follow motion of control interface
Position Task (PT)	Low	Resist haptic moments and maintain position of control interface

D. NMS related tuning choices

The following choices for neuromuscular stiffness, and thereby the tuning of the haptic feedback, can be distinguished:

1) Intrinsic (relax task) stiffness: The haptic feedback is tuned to match the intrinsic stiffness of the operator's NMS, i.e., the haptic feedback moment is scaled such that when applied, it will move operator's relaxed arm holding the stick to the 'optimal stick position'. The haptic feedback will result in the correct stick response, unless the operator stiffens up, *actively disagreeing* with the guidance. The advantage of this tuning is that the physical work of the operator is minimized; for the intrinsic stiffness the Golgi tendon organ and muscle spindle feedback paths are not used. In many cases the spring stiffness of the stick will be higher than the intrinsic stiffness of the human operator. Consequently, the stick stiffness alone will not be too different from the combined stiffness of the stick and hand, and so the this tuning will also produce an acceptable response for a hands-off control.

2) Lower than intrinsic stiffness: The haptic feedback is tuned to match a lower than intrinsic stiffness of the NMS of the operator [18] (with force task stiffness being the lower limit). Such tuning keeps the operator more involved in the control loop by requiring active NMS adaptation towards the force task, which can be described as requiring *active*

agreement. Interestingly, even negative stiffness tuning has been used in literature: to encourage fast evasive maneuvers in a car driving support system [23].

3) Higher than intrinsic stiffness: The haptic feedback is tuned to match a higher than intrinsic stiffness of the NMS (with position task stiffness being the upper limit). The haptic guidance moment would result in correct stick position if the operator maintains increased arm stiffness, otherwise the stick position response to the haptic guidance will be too large, leading to overshoots during the avoidance maneuvers [17]. Depending on the actual tuning, it can be difficult for the operator to overrule the haptic feedback.

In this paper, we advocate the choice of using intrinsic stiffness as the reference in tuning the collision avoidance HSC, for three reasons. First, intrinsic stiffness based tuning ensures that the physical workload of the operator is minimized, since no muscular activity is required to maintain intrinsic stiffness. Second, the system prevents colliding, unless the operator *actively disagree* by stiffening up the arm. And third, this setting has the attractive property that when the stick is released, the UAV will steer away from nearby obstacles.

E. Identifying intrinsic neuromuscular system admittance

The NMS properties of human subjects are typically determined in three fundamental tasks, Table I [24]. The intrinsic stiffness of the neuromuscular system can be directly determined in the relax task, in which the reflexes are not used and the arm dynamics are dominated by its visco-elastic properties. However, the UAV control stick is normally spring centered, requiring the operator, in order to command UAV motion, to deflect the stick by applying force on it. The intrinsic NMS properties therefore need to be determined in presence of a bias force. Unfortunately, it is unattainable for subjects to maintain the required bias force and simultaneously suppress their neural reflexes to correctly execute the relax task. A method to overcome this practical challenge and identify the intrinsic NMS in a force task is described in the next section.

III. Neuromuscular identification experiment

The identification of human neuromuscular properties traditionally relies on using multisine signals to provide excitation forces on a range of frequencies. However, the distribution of power over the frequencies influences the reflexive action of the NMS [25]. A novel identification method, described in detail in a previous study [7], uses a disturbance signal with a wide-band spectrum, to suppress the arm's natural reflexes. In this manner the adaptation range of the NMS is effectively limited to the intrinsic visco-elastic properties.

A. Method

1) Subjects and task instructions: Ten subjects (three female), all staff or graduate students of TU Delft, with an average age of 28.6 years ($\sigma = 2.4$) performed the experiment. All subjects were right-handed, none reported injuries or any other disorder in the upper extremities. The experiment was approved by the Delft University of Technology Human Research Ethics Committee. Subjects gave their informed consent prior to the experiment and no monetary compensation was offered.

The subjects were seated in an adjustable chair, Fig. 3, such that the right forearm was parallel with the roll axis of the stick. The stick's hardware casing served as a rest for the forearm. Subjects were asked to perform force task, Table I, keeping constant grip and hand position during the experiment.

2) Experiment design and procedure: Three levels of bias moment magnitude were tested, 0, 0.7 and 1.4 $[\mathrm{Nm}]$, in six directions: $0°$, $45°$, $90°$, $135°$, $180°$, and $270°$; constituting thirteen test conditions $C_{1..13}$. A wide-band test signal (Section III-A4), applied as an additional moment on the stick, was used. Both, as a means of excitation to be able to identify the NMS, and to ensure that the reflex feedback action is suppressed. The experiment lasted approximately 1.5 hours, including briefing, debriefing, familiarization runs, and breaks.

The experiment started with performing multiple training runs to familiarize the subjects with the tasks. After that three experimental runs were done for all 13 conditions. Each individual run lasted 60 seconds, consisting of 10 seconds run-in time and of approximately 50 seconds measurement time, resulting in 9 full periods of the test signal for every condition.

3) Apparatus: The electro-hydraulic side stick with armrest (A), in Fig. 3, is located to the right of an adjustable chair. An 18 inch display, (B), was located at a distance of 80 cm in front of the subject. The side stick could move with two degrees of freedom, in pitch and roll rotation. The effective length, from axis of rotation to the center of the hand, between the middle and index finger, was $0.09\,[\mathrm{m}]$ and the motion range was $\pm 22°$ for pitch and $\pm 30°$ for roll motion. The side stick measured the stick angular displacement $\underline{\delta}_{st}(t) = \left[\delta_{st_p}(t),\, \delta_{st_r}(t)\right]^T$, the handling moment $\underline{m}(t) = \left[m_p(t),\, m_r(t)\right]^T$ applied by the subject on the stick, and the disturbance moment $\underline{d}(t) = \left[d_p(t),\, d_r(t)\right]^T$ imposed on it, for both roll and pitch respectively. Signals were sampled at 250 Hz. The active side stick was controlled to behave as a mass-spring-damper system, as:

$$H_{st}(s) = \frac{\underline{\delta}_{st}(s)}{\underline{m}(s)} = \frac{1}{I_{st}s^2 + B_{st}s + K_{st}}, \tag{2}$$

where, for both the pitch and roll directions, inertia of $I_{st} = 0.02\,[\mathrm{kg\,m^2}]$, damping coefficient $B_{st} = 0.2\,[\mathrm{Nms\,rad^{-1}}]$ and spring coefficient $K_{st} = 2\,[\mathrm{Nm\,rad^{-1}}]$ were used.

4) Disturbance signal design: Two uncorrelated multi-sine signals $d_p(t)$ and $d_r(t)$ were designed in the frequency domain to excite the stick-arm dynamics in pitch and roll directions. Both signals contained power at 20 logarithmically distributed frequencies, $\underline{f} = \left[f_p,\, f_r\right]^T$, within a range of $0.4\,\mathrm{Hz}$ and $20\,\mathrm{Hz}$, Fig. 4a. The phases were selected to minimize the crest factor (peak-to-average amplitude ratio) [26]. Figure 4b shows one period ($16.38\,\mathrm{s}$) of the disturbance signal in the time domain [27].

The signals had full power between $0.4\,\mathrm{Hz}$ and $2.5\,\mathrm{Hz}$ and 20% of the power above that frequency. A standard approach in human NMS admittance identification literature is to use the full power signal only approximately below 1 Hz (reduced power method [25]). In contrast, in this work, the full power signal was intentionally applied above this frequency, to actually *suppress* the natural reflexes of the operator's arm, and

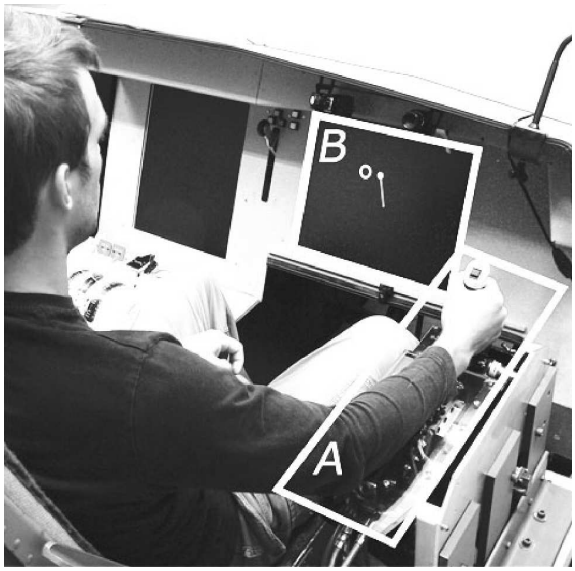

Fig. 3. Neuromuscular identification experiment setup. The subject used the stick (A), to control position of a white dot on the display (B).

allow the identification of intrinsic admittance. Alternatively, a uniform power distribution over all disturbance frequencies could have been used, or the higher frequencies could be omitted altogether in the future identification experiments, since these are not needed for the presented tuning method.

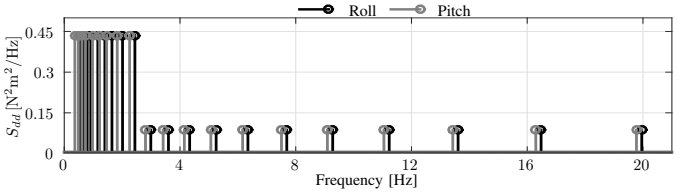

(a) Perturbation signal designed in frequency domain.

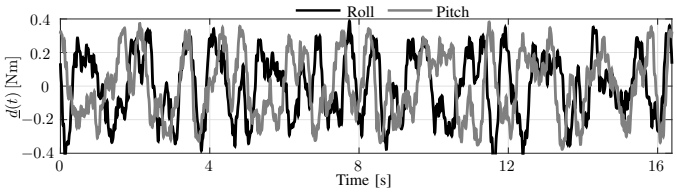

(b) One complete period (16.38 s) of the disturbance signal.

Fig. 4. Disturbance signal. Frequency and time domain content of the disturbance moment realizations for roll and pitch.

5) Experimental data pre-processing: As a first step, mean values were subtracted from the measured time domain signals, ($\underline{d}(t)$, $\underline{\delta}_{st}(t)$ and $\underline{m}(t)$). Then the repetitions over the same condition were averaged in the time domain to reduce measurement noise and non-linear behavior of the NMS (e.g., voluntary inputs, muscle fatigue).

6) Admittance estimation using spectral analysis: The moment input $\underline{m}(t)$, disturbance input $\underline{d}(t)$ and stick angle output $\underline{\delta}_{st}(t)$ were used to estimate auto- and cross-spectral densities $S_{\delta_{st}d}(\underline{f})$ and $S_{md}(\underline{f})$ at the frequencies of the disturbance signal $\underline{f}$. The NMS admittance is then obtained by using a closed-loop identification method [28].

Because the disturbance moment inputs are uncorrelated, the multiple-input and multiple-output admittance can be evaluated by using four separate single-input and single-output spectral estimators [27], [29]. The admittance is calculated separately for all thirteen conditions ($C_{i=1..13}$):

$$\hat{G}_{C_i}(\underline{f}) = \begin{bmatrix} \frac{S_{\delta_{st_p}d_p}(\underline{f}_p)}{S_{m_pd_p}(\underline{f}_p)} & \frac{S_{\delta_{st_p}d_r}(\underline{f}_r)}{S_{m_rd_r}(\underline{f}_r)} \\ \frac{S_{\delta_{st_r}d_p}(\underline{f}_p)}{S_{m_pd_p}(\underline{f}_p)} & \frac{S_{\delta_{st_r}d_r}(\underline{f}_r)}{S_{m_rd_r}(\underline{f}_r)} \end{bmatrix} \tag{3}$$

7) Endpoint admittance ellipse: An intuitive way to visualize the 2-DOF dynamic characteristic of the endpoint admittance is using admittance ellipses [24]. The admittance ellipse displays the magnitude and direction of the response of the NMS to a unit moment input and is characterized by the size and direction of its major and minor axes. The major axis of the ellipse corresponds to the direction of the NMS with the least resistance to moment disturbances (highest admittance), and the minor axis to the direction with the largest resistance. The admittance ellipse can be evaluated at frequencies of the disturbances $f \in \underline{f}$ by:

$$\begin{bmatrix} \delta_{ell_r} \\ \delta_{ell_p} \end{bmatrix} = |\hat{G}_{C_i}(f)| \begin{bmatrix} \cos(\alpha) \\ \sin(\alpha) \end{bmatrix}, 0 \leq \alpha \leq 2\pi, \tag{4}$$

where δ_{ell_r} and δ_{ell_p} are the endpoint rotations for roll and pitch to unit moment disturbances, respectively.

B. Results

The endpoint admittance ellipses at a low frequency ($f = 0.5$ Hz) for all conditions averaged over all subjects are shown as in Fig. 5 (standard deviation is displayed in light gray). Data of one subject were discarded due to its very low admittance indicating incorrect execution of the requested task. Presented experimental data are publicly available online [30].

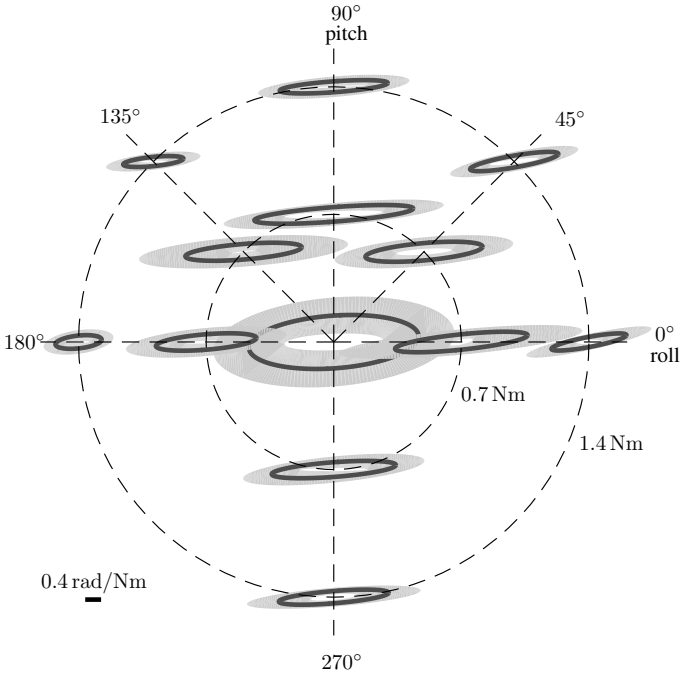

Fig. 5. Mean estimated admittance ellipses over all subjects at $f = 0.5$ Hz. The standard deviation, shown in light gray, indicates relatively high consistency in responses among the group of subjects.

IV. UAV TELEOPERATION EXPERIMENT

The set of NMS admittance measurements, previously obtained in Section III, is in this section used as a reference for tuning a HSC collision avoidance system, and evaluated in a human study with a teleoperated UAV control task.

A. UAV Teleoperation

1) UAV model: The UAV was modeled as an 'easy-to-fly', control-augmented, helicopter with a rotor diameter of 3 [m] [14]. Longitudinal side-stick inputs δ_p were mapped to forward velocity commands V_x, whereas lateral inputs δ_r were mapped to yaw rate commands $\dot{\psi}$, which is not uncommon for, e.g., stabilized quadrotors:

$$H_{\text{UAV}_x}(s) = \frac{V_x(s)}{\delta_p(s)} = \frac{1}{(0.3s+1)(0.18s+1)} \qquad (5)$$
$$H_{\text{UAV}_y}(s) = \frac{\dot{\psi}(s)}{\delta_r(s)} = \frac{1}{(0.2s+1)}$$

In addition to the above dynamics, the UAV has a maximum velocity, V_{max}, and acceleration, a_{max}, of 5.0 [m/s] and 1.0 [m/s^2] in the longitudinal direction, and a maximum yaw rate, $\dot{\psi}_{max}$, and yaw acceleration, $\ddot{\psi}_{max}$, of 0.32 [rad/s] and 2.0 [rad/s^2] in the lateral direction. The UAV altitude was kept constant by an autopilot.

2) Environment: Six obstacles, modeled as buildings of different shapes, see Fig. 6, made up the virtual environment of the remote sensing task (the environment was also used in previous studies [14]). Each obstacle was designed to evoke different control behavior. For instance, obstacle 3 required subjects to fly backwards into a U-shape building, with no visual cues in the direction of motion. Obstacles were re-arranged to create three different measurement and three training trajectories, to reduce boredom and learning effects.

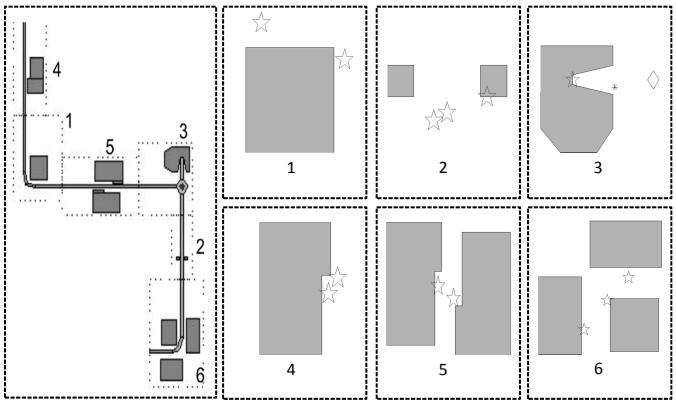

Fig. 6. An example of a virtual environment composed of six obstacles; with waypoints (star symbols) to be flown through. A path to be flown backwards (diamond) ends inside the obstacle 3 opening (visually marked by an asterisk).

3) Parametric risk field: The parametric risk field (PRF) is the component of the automatic controller responsible for mapping obstacles in the environment to the optimal collision avoidance side-stick inputs, see Fig. 1. The risk field is computed in the UAV reference frame, expressing the risk of collisions for obstacles detected within the scanned area. Subsequently, in Section IV-A4, the corresponding repulsive haptic moments are calculated and applied on the side-stick by the haptic controller to help the teleoperator to steer away from possible collisions. The PRF [16], was specifically designed for UAV teleoperation. It was found to generate more stable haptic moments, when compared to other haptic collision avoidance fields discussed in literature [15], [16], [31].

The shape and size of the risk field is proportional to the instantaneous UAV velocity, $\mathbf{v}$, and inversely proportional to its maximum deceleration, a_{max}. If the UAV is stationary, the field spans only a small circular region around the UAV. For non-zero velocities, the field extends in the direction of motion to provide sufficient time for the teleoperator to react to the haptic cues. Fig. 7 displays the parameters and zones that define the PRF. Parameters d_{stop} and d_{ahead} are responsible for extending the size of the field when the UAV is moving and are defined as [14]:

$$d_{stop} = \frac{|\mathbf{v}|^2}{2a_{max}} \qquad d_{ahead} = |\mathbf{v}|\, t_{ahead} \qquad (6)$$

The risk field geometry is defined by four constant parameters: r_{pz}, d_{min}, t_{ahead} and a_{max}. The values of these parameters were refined through simulations for the UAV model used in this research by Lam et al. [16] and are listed in Table II. The risk of collision, R, is based on the relative distance between the UAV and an obstacle, $\mathbf{p}$, also taking in account the instantaneous UAV velocity, $\mathbf{v}$:

$$R(\mathbf{p},\mathbf{v}) = \begin{cases} 1 & \text{if } \mathbf{p} \text{ in Zone 1} \\ \cos\left(\frac{d}{d_0}\frac{\pi}{2} + \frac{\pi}{2}\right) + 1 & \text{if } \mathbf{p} \text{ in Zone 2} \\ 0 & \text{if } \mathbf{p} \text{ in Zone 3} \end{cases} \qquad (7)$$

The cosine function for risk computation in Zone 2 enables a smooth transition in risk values between zones, consequently ensuring that there will be no sudden changes in the applied haptic moments. To evaluate the risk at point $\mathbf{p}$, distances d and d_0 need to be computed, see Fig. 7.

The risk is used to compute an optimal side-stick input δ^*_{st}. First, the magnitude of the risk is calculated using Eq. (7), and its direction is defined from the obstacle to the center of the UAV. This allows for a straightforward implementation if a discrete sensor spanning the 360° area around the UAV is used [16]. If multiple obstacles are detected, the final collision avoidance steering vector is computed by vectorially summing the largest and smallest collision avoidance steering vectors, using the 'max-min' method [14]. Second, the resulting risk vector is scaled to the physical input limits of the side-sticks (for details see Section III-A3), i.e., the maximal risk value corresponded to the maximal deflection of the side-stick.

TABLE II
PARAMETRIC RISK FIELD PARAMETERS.

Parameter	Value	Description
r_{pz}	1.5	Radius of protection zone [m]
d_{min}	1.5	Distance between zone 1 and zone 2 [m]
t_{ahead}	2	Maximum available reaction time [s]
a_{max}	1	Maximum UAV deceleration $[m/s^2]$

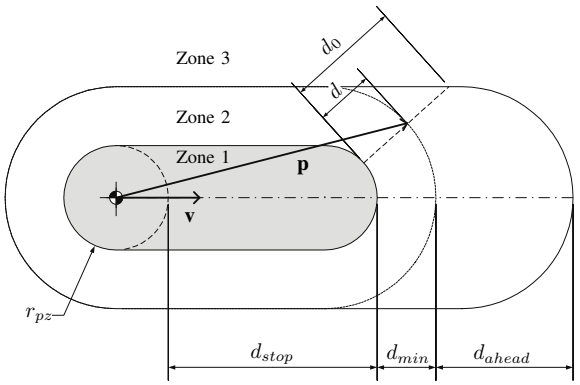

Fig. 7. Parametric risk field. Variables used to describe the shape of the parametric risk field (based on [14]).

4) Haptic controller implementation: The haptic controller (HC) was implemented using the averaged admittance of ten subjects measured in Section III, at a measurement/excitation signal frequency of 0.5 Hz. As discussed in Section II, admittance depends on the magnitude and direction of manual control inputs [7], [32]. To account for this, the tuning was determined for 13 different conditions, as is shown in Fig. 5. The control law relating the optimal side-stick position δ_{st}^* (based on the risk calculated by Eq. (7) to the applied haptic moment, M_G, was implemented according Eg. (1).

The motions of the UAV with respect to the obstacles in the surroundings, and thereby the fluctuations in the haptic feedback, will produce signals from the collision avoidance system that are generally lower in bandwidth than 1 Hz [14]. Based on the estimated frequency responses, the combination of the NMS and the control interface can be for design purposes considered to be a constant gain [7]. The admittance at a low frequency ($f = 0.5$ Hz) over all conditions $C_{1..13}$ was transformed to stiffness:

$$\mathbf{K_{NMS}}(\delta_{st}) = \left(\hat{G}_{C_i}(f)\right)^{-1} \tag{8}$$

To account for all permissible stick inputs δ_{st}, nearest neighbor interpolation was used to compute appropriate haptic cues (i.e., the closest available $\mathbf{K_{NMS}}(\delta_{st})$ to the instantaneous teleoperator manual control input is selected). The mapping of the instantaneous stick position δ_{st} to the $\mathbf{K_{NMS}}(\delta_{st})$ stiffness gains is visualized in Fig 8. It is hypothesized that this stick position-depended tuning approach will allow the haptic controller to better account for adaptation in NMS (in contrast to using only one constant NMS stiffness value), and as a consequence, improve the teleoperator's appreciation of the haptic cues.

By visual inspection of the identified admittance ellipses, Fig. 5, a small roll-pitch and pitch-roll cross-term effect (i.e., rotation of the admittance ellipses) was observed. However, it was deemed undesirable for the guidance forces to utilize this cross coupling and so to prevent it, the corresponding stiffness cross-term gains were set to zero, as: $\mathbf{K_{NMS}}(\delta_{st}) = \begin{bmatrix} K_{\mathrm{NMS}_p} & 0 \\ 0 & K_{\mathrm{NMS}_r} \end{bmatrix}$.

B. Method

1) Subjects and task instructions: Twelve right-handed male subjects, all graduate students of TU Delft, with an average age of 23.4 years ($\sigma = 0.7$), took part in the experiment. None of the subjects participated in the previous identification stage and none had any prior experience with haptic interfaces. Subject gave consent prior to the experiment and no monetary compensation was offered. The experiment was approved by the Delft University of Technology Human Research Ethics Committee.

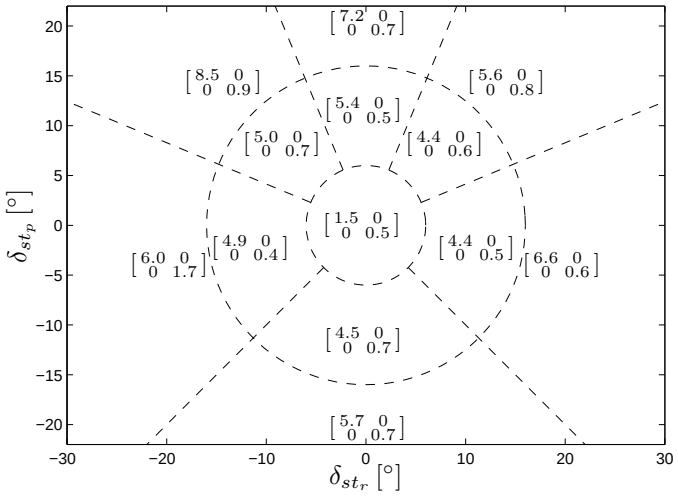

Fig. 8. Mapping of actual stick position δ_{st} to the tuning gain $\mathbf{K_{NMS}}(\delta_{st})$ $\left[\mathrm{Nm\ rad}^{-1}\right]$.

During the experiment, subjects performed a UAV surveillance task in an obstacle laden urban environment. Subjects were instructed, in order of priority to: 1) avoid collisions, 2) fly as closely as possible through the center of waypoints (represented as smoke plumes), and 3) to perform the task as fast as possible. To improve experiment realism, each collision resulted in a 20 second time penalty during which the experiment was paused. Each trial took approximately 150 seconds to complete (when flown without collisions).

2) Apparatus: A fixed-base flight simulator was used to perform the experiment, see Fig. 9. Subjects were seated in a pilot chair (1) and used the same electro-hydraulic side-stick with the same dynamical parameters as in the preceding NMS admittance identification experiment. The side-stick (2) was used to manually control the UAV through the environment. Visual cues of the surroundings were projected on a wall in front of the subject, originating from a simulated onboard camera fixed to the longitudinal forward axis of the UAV (4). Additionally, a top-down view display was provided to aid the operator with navigating around obstacles (3).

3) Independent measures: Two categories of independent variables were studied in the experiment. The first category was concerned with the tuning profile (TP) of the haptic controller. A total of four TPs were tested, resulting in the four experiment conditions listed in Table III. Here, UT and OT controllers represent TPs that are half and twice as strong as RT tuning, respectively. These two TPs were defined to study the sensitivity of the novel tuning procedure.

The second independent variable was obstacle (OB). Six different obstacles were tested during the experiment and the subjects were required to fly through all of them in every trial, for details see Section IV-A2.

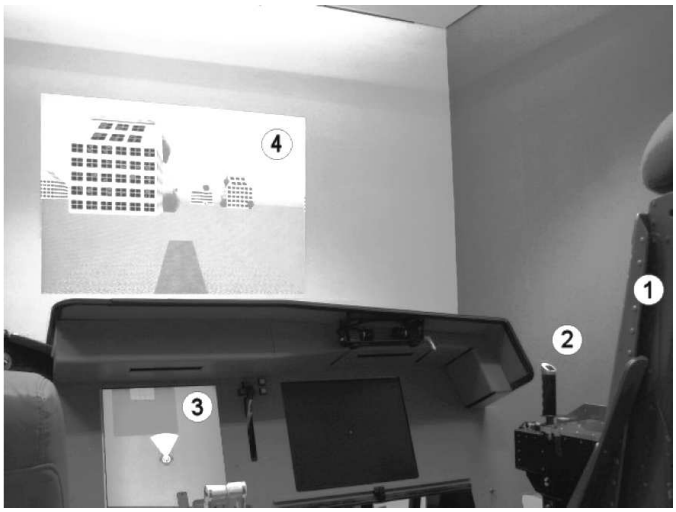

Fig. 9. UAV teleoperation experiment setup. Fixed-base flight simulator with aircraft chair (1), hydraulic side-stick (2), navigation display (3) and onboard camera view (4).

TABLE III
UAV TELEOPERATION EXPERIMENT CONDITIONS AND COLOR CODING.

Color	Symbol	Description
	NHF	No haptic feedback / pure manual control
	UT	HSC under-tuned relative to RT (UT=0.5RT)
	RT	HSC tuned based on relax task admittance data collected in Section III
	OT	HSC over-tuned relative to RT (OT=2RT)

4) Dependent measures: The dependent measures used to compare the different haptic controllers can be divided into six categories: safety, performance, control activity, haptic activity, haptic controller agreement and subjective questionnaires. They are listed in Table IV. To assess the agreement between the operator's voluntary moment inputs, M_H, and the haptic guidance moment, M_G, two separate metrics were calculated. The metrics were calculated in discrete time, for times when the haptic controller was active, i.e., for all k when $|M_G(k)| > 0$. Magnitude comparisons are based on the RMS error between the magnitudes of measured moment and the haptic moment as:

$$M_{\text{rms}} = \sqrt{\frac{1}{n}\sum_{k=1}^{n}\left(|M_G(k)| - |M_H(k)|\right)^2}, \tag{9}$$

with smaller values indicating higher magnitude agreement. Directional agreement is assessed as the ratio of haptic and measured moments having the same sign as:

$$M_{\text{sgn}} = \frac{1}{n}\sum_{k=1}^{n}\text{eql}\left(\text{sgn}(M_G(k)), \text{sgn}(M_H(k))\right), \tag{10}$$

where operator $\text{eql}(a, b)$ equals 1 if $a = b$, otherwise it equals 0. A M_{sgn} value of 1 indicates perfect agreement, whereas a value of 0 indicates total disagreement of moment directions.

The control activity, haptic activity, and haptic controller agreement were analyzed separately along the pitch (p) and the roll (r) axes to investigate the control strategy differences between the two directions observed during a pilot study.

TABLE IV
EXPERIMENT DEPENDENT MEASURES.

Measure	Symbol	Description
Safety	$n_{collisions}$	Number of collisions [-]
Performance	$\overline{V}$	Mean velocity [m/s]
	d_{wp}	Minimum distance to waypoints [m]
Control Activity	$\sigma_{\dot{\delta}}$	Standard deviation of stick rate [rad/s], both roll and pitch
Haptic Activity	σ_{M_G}	Standard deviation of haptic guidance moment [Nm], both roll and pitch
Haptic Controller Agreement	M_{rms}	RMS error between the magnitude of human applied moment and the haptic guidance moment [Nm]
	M_{sgn}	Ratio of haptic guidance and human applied moments having the same sign [-]
Subjective	NASA TLX	Workload assessment survey
	SA	Situational awareness survey
	HA	Haptic feedback acceptance survey

Questionnaires were used to measure subjective workload, situational awareness (SA) and haptic feedback acceptance (HA). Workload is measured using the NASA Task Load Index (TLX) questionnaire [33]. The NASA TLX calculates workload as the weighted average of six subjective sub-scales: mental demand, physical demand, temporal demand, performance, frustration and effort. A higher weighted average (ranging between 0 and 100), suggests higher subjective workload. SA and HA are measured using questionnaires similar to the Eurocontrol SASHA method [34]. These questionnaires capture the teleoperators' awareness of their surroundings and whether haptic feedback was subjectively helpful in completing the task, respectively. The SA and HA questions are answered on a five point Likert type scale (ranging between 0 and 4), and the mean score of all the questions is taken as the measure of SA and HA, with higher scores indicating higher SA/HA.

5) Hypotheses: Three hypotheses were formulated for the validation experiment. Firstly, we hypothesized that task *safety*, in accordance with previous research [15], [16], will be increased with stronger *tuning profile* of the haptic controller.

Secondly, the task *performance* would remain unaffected by the *tuning profiles*, since the haptic cues should ideally not interfere with the task and only prevent collisions.

Thirdly, the *workload* associated with the task and the *acceptance of haptic feedback* should be optimal for the RT.

6) Procedure: The experiment began with three initial training to allow subjects to practice controlling the UAV with and without the aid of haptic cues. Afterward, subjects flew one additional training run and four measurement runs for each TP. Experiment conditions were randomized and subjects had no prior knowledge of the conditions performed. At the end of each condition, subjective workload (using NASA TLX), situational awareness and haptic feedback acceptance were measured using questionnaires. The total duration of the

experiment, including briefing, debriefing, familiarization runs, and breaks, was approximately 2 hours.

7) Data analysis: All objective dependent measures were computed per obstacle to take into account the different order of obstacles in each trajectory. The effects of the independent variables (TP and OB) on the dependent measures were analyzed using two-way repeated-measures ANOVA, with pairwise Bonferroni corrected comparisons used as post-hoc tests. For non-spherical data the Greenhouse-Geisser corrections were applied to the degrees of freedom [35].

Ordinal dependent measures, $n_{collisions}$ and subjective questionnaires results, were evaluated using the Friedman test; with Bonferroni corrected Wilcoxon signed-rank test as post-hoc.

8) Visualization of results: Results are shown using their means and the 95% confidence intervals of the mean. The color coding of tuning profiles follows Table III. Questionnaire results are visualized as box-plots, showing the median, the 25th and 75th percentiles and the maximal and minimal values (excluding outliers) over all subjects.

Due to the low number of collisions, the $n_{collisions}$ were summed over all subjects; corresponding confidence intervals (95%) are bootstrapped using the bias-corrected and accelerated percentile method (BCa) with 5000 samples [35].

C. Results

The experimental results are in this section presented separately for all studied dependent measures. Overall, after the initial training period, there were no learning effects observed in the experimental data.

1) Safety: Fig. 10a shows that the total number of collisions, $n_{collisions}$, decreased with increasing strength of the haptic controller, and was the lowest for the OT condition. However, the Friedman test did not reveal a significant effect of TP on $n_{collisions}$ (TP: $\chi^2(3) = 7.48$, $p = 0.058$).

The Friedman test did show an effect of OB on $n_{collisions}$, Fig. 10b, (OB: $\chi^2(5) = 17.31$, $p \leq 0.01$). Obstacle 5, which resulted in the highest number of collisions, was also reported by subjects to be the most difficult.

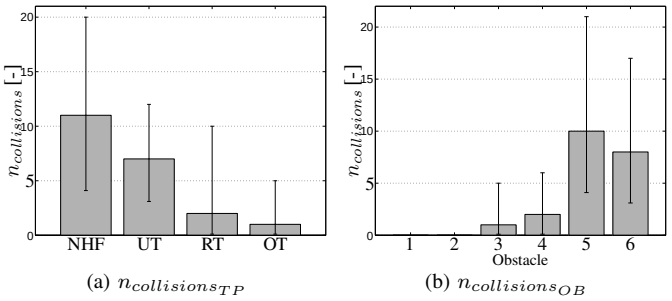

(a) $n_{collisions_{TP}}$ (b) $n_{collisions_{OB}}$

Fig. 10. Task safety evaluated separately as a total number of collisions for all tuning profiles TP and obstacles OB over all subjects.

2) Performance: The mean velocity of the UAV, $\overline{V}$, is shown in Fig. 11a. Here it can be seen that for a particular obstacle, $\overline{V}$ was relatively constant for all haptic controllers. On the other hand, $\overline{V}$ did vary substantially with OB, a significant effect (OB: $F_{2.39,26.29} = 107.16, p \leq 0.01$). When comparing Fig. 11a with Fig. 10b, it can be seen that velocity tends to be lower for obstacles with a higher number of collisions. This indicates that subjects decreased UAV velocity in an attempt to follow the primary task instruction of avoiding collisions, particularly for difficult obstacles.

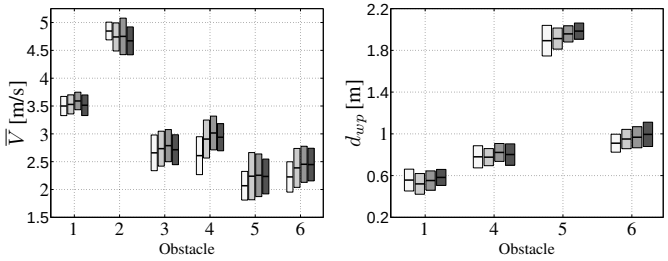

(a) $\overline{V}$ (b) d_{wp}

Fig. 11. Task performance. Obstacles 2 and 3 did not have smoke plumes serving as waypoints. TP coding is described in Table III.

Similar to $\overline{V}$, the minimum distance to waypoints, d_{wp}, was not influenced by TP, but affected by OB (OB: $F_{3,33} = 296.79, p \leq 0.01$), see Fig. 11b. Moreover, it can be seen that d_{wp} followed the same trend as $n_{collisions_{OB}}$ and obstacles with more collisions had higher d_{wp}. This provides additional evidence that subjects employed a conservative control strategy when tackling difficult obstacles.

3) Control activity: The standard deviation of the longitudinal side-stick deflection rate, $\sigma_{\dot{\delta}_p}$, is shown in Fig. 12a. For all obstacles, $\sigma_{\dot{\delta}_p}$ was the smallest for NHF and the largest for OT (TP: $F_{1.33,14.59} = 19.56, p \leq 0.01$). The roll stick deflection rate $\sigma_{\dot{\delta}_p}$ was the lowest for obstacle 2 (OB: $F_{1.93,21.27} = 42.80, p \leq 0.01$).

In the lateral direction, Fig. 12b, $\sigma_{\dot{\delta}_r}$ was the highest for the OT controller (TP: $F_{3,33} = 17.57, p \leq 0.01$). Similar to the longitudinal direction, post-hoc tests revealed no differences between UT and RT for $\sigma_{\dot{\delta}_r}$. Since turning was not necessary to complete obstacle 2, this obstacle resulted in the lowest $\sigma_{\dot{\delta}_r}$ (OB: $F_{1.93,21.27} = 25.95, p \leq 0.01$).

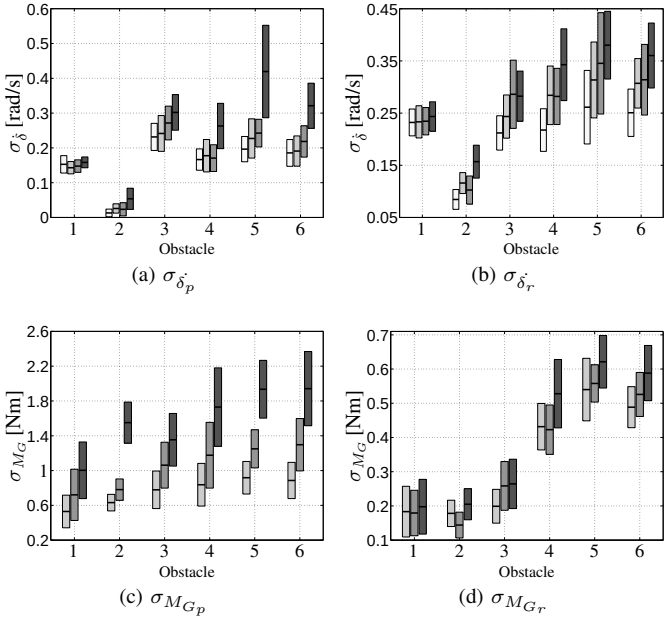

(a) $\sigma_{\dot{\delta}_p}$ (b) $\sigma_{\dot{\delta}_r}$

(c) $\sigma_{M_{G_p}}$ (d) $\sigma_{M_{G_r}}$

Fig. 12. Control and haptic activity. Coding is described in Table III.

4) Haptic activity: The standard deviation of the longitudinal haptic guidance moment, $\sigma_{M_{G_p}}$, shown in Fig. 12c, increased with increasing strength of the haptic controller (TP: $F_{1.35,14.87} = 75.88, p \leq 0.01$). Post-hoc tests showed differences between all three haptic controllers ($p \leq 0.01$). In terms of OB, variations increased from obstacle 1 to 6 (OB: $F_{2.66,29.24} = 6.50, p \leq 0.05$).

Standard deviation of the lateral haptic guidance moment, $\sigma_{M_{G_r}}$, are much greater for obstacles 4-6 when compared to obstacles 1-3 (OB: $F_{2,22} = 9.57, p \leq 0.01$), see Fig 12d. The OT tuning produced the largest $\sigma_{M_{G_r}}$ for all obstacles (TP: $F_{2,22} = 9.57, p \leq 0.01$). Post-hoc tests showed no differences between UT and RT controllers.

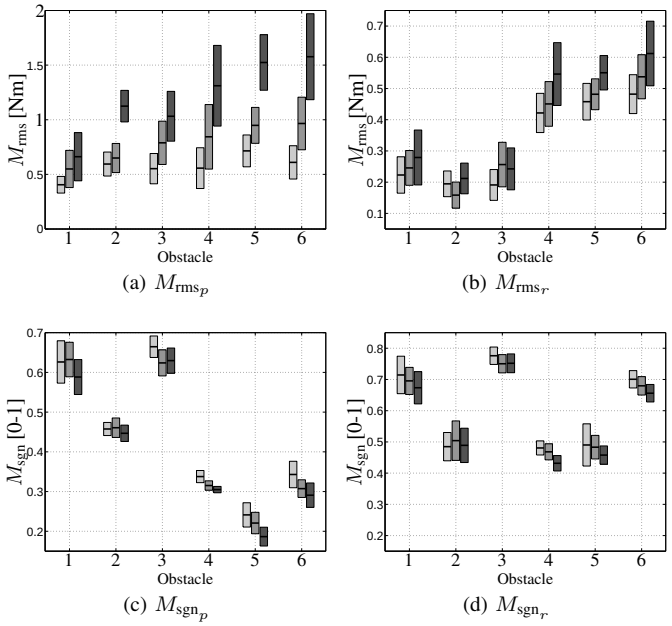

(a) M_{rms_p} (b) M_{rms_r} (c) M_{sgn_p} (d) M_{sgn_r}

Fig. 13. Haptic controller agreement. Coding is described in Table III.

5) Haptic Controller Agreement: Longitudinal agreement of the haptic moment magnitude, M_{rms_p}, is shown in Fig. 13a. OT was found to have the highest value for M_{rms_p}, and consequently the lowest magnitude agreement of all controllers (TP: $F_{1.70,18.67} = 49.35, p \leq 0.01$). With respect to OB, obstacle 1 resulted in highest magnitude agreement while it was lowest for obstacle 6 (OB: $F_{2.24,24.55} = 5.45, p \leq 0.01$). As the differences between controllers is more evident for obstacles 4-6, a two-way interaction was also observed (TP×OB: $F_{3.59,39.53} = 10.99, p \leq 0.01$).

For the haptic moment magnitude agreement in the lateral direction, M_{rms_r}, in Fig. 13b, OT had the lowest lateral magnitude agreement (TP: $F_{4,44} = 13.17, p \leq 0.01$). When compared to the longitudinal direction, magnitude agreement is higher for M_{rms_r}. However, variations between controllers increase for obstacle 4-6 yielding a significant two-way interaction (TP×OB: $F_{20,220} = 2.124, p \leq 0.01$), and as these three obstacle also caused lower magnitude agreement (SB: $F_{5,55} = 46.36, p \leq 0.01$).

Directional agreement of longitudinal haptic moments is assessed using M_{sgn_p}, in Fig. 13c, with larger values implying greater agreement. Highest directional agreement was found for UT, and the lowest for OT, resulting in a significant effect of TP on M_{sgn_p} (TP: $F_{4,44} = 26.35, p \leq 0.01$). Obstacle 1 and 3 exhibited high directional agreement, but agreement was fell sharply for obstacles 4-6 (OB: $F_{5,55} = 231.75, p \leq 0.01$).

Lateral directional agreement, M_{sgn_r}, is shown in Fig. 13d. It can be seen that lateral directional agreement is, on average, greater than for the longitudinal direction. Obstacle 3 resulted in the highest lateral directional agreement as the UAV was required to fly backwards, forcing subjects to rely on haptic cues to avoid obstacles outside their lateral field of view. Obstacles 1 and 6 also resulted in much higher directional agreements than other obstacle as these two obstacles involved sharp 90^o turns which, while making the turn, obscured visual position of obstacles. These findings yield a significant effect of OB on M_{sgn_r} (OB: $F_{5,55} = 76.813, p \leq 0.01$). Concerning the relationship with TP, lateral directional agreement deteriorated with increasing strength of the haptic controller (TP: $F_{4,44} = 10.38, p \leq 0.01$).

6) Subjective questionnaires: Fig. 14a displays overall workload, or Z-score, computed using the NASA TLX subjective questionnaire. Here a lower subjective rating symbolizes lower workload. The Friedman test showed that there was an effect of TP on overall workload (TLX: $\chi^2(3) = 18.10$, $p \leq 0.01$). Post-hoc analysis revealed that the differences were caused by the extreme conditions, NHF and OT, which had the highest workload levels. However, no substantial differences were recorded between UT and RT, and these two controllers led to the lowest measured workload. The six

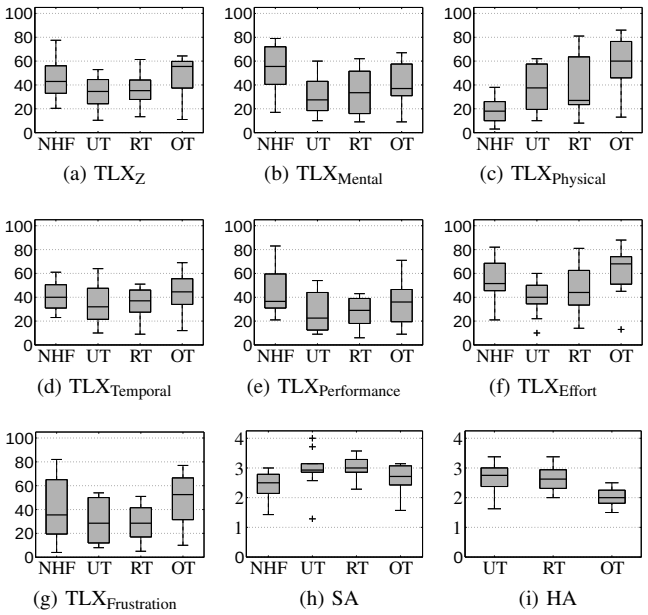

(a) TLX_{Z} (b) $\text{TLX}_{\text{Mental}}$ (c) $\text{TLX}_{\text{Physical}}$ (d) $\text{TLX}_{\text{Temporal}}$ (e) $\text{TLX}_{\text{Performance}}$ (f) $\text{TLX}_{\text{Effort}}$ (g) $\text{TLX}_{\text{Frustration}}$ (h) SA (i) HA

Fig. 14. Subjective metrics: NASA TLX, Situational Awareness (SA), and Haptic Acceptance (HA).

workload sources of the NASA TLX are pictured in Figs. 14b to 14g. Mental load (ML) and effort (EF) for UT/RT were reduced compared to NHF (ML: $\chi^2(3) = 16.20$, $p \leq 0.01$; EF: $\chi^2(3) = 15.91$, $p \leq 0.01$). However, physical load (PL) continued to be higher for the novel tuning method, and increased with the strength of the haptic controller, a significant effect (PL: $\chi^2(3) = 25.23$, $p \leq 0.01$). Despite improvements in performance, frustration and temporal load

for UT/RT, TP effects were not significant.

Box plots for subjective situational awareness (SA) and haptic feedback acceptance (HA) are given in Figs. 14h and 14i. Here, higher subjective ratings imply better SA and HA. A Friedman test showed an effect of TP on SA, with the highest and lowest median SA recorded for RT and NHF respectively (SA: $\chi^2(3) = 11.58$, $p \leq 0.01$). A similar trend was found for HA, with the highest acceptance for UT and RT, and the lowest for OT (HA: $\chi^2(2) = 8.21$, $p \leq 0.05$).

V. Discussion

The main objective of this study is to provide a systematic and validated approach for tuning Haptic Shared Control (HSC) systems based on estimated admittance of the neuromuscular system (NMS), and – more specifically – to advocate the choice of the relax task admittance as the setting with the minimal required operator workload. To this end, a human-in-the-loop experiment simulating UAV teleoperation was performed to validate the tuning procedure. The following effects were observed:

NMS based tuning works as a systematic method

In general, subjective workload and situational awareness improved significantly for the under-tuned and the relax-task tuned haptic controllers when compared to manual control. Additionally, over-tuning the haptic controller, as is might be the case for heuristic tuning methods optimizing for safety [14], yields lower user acceptance than the condition with no haptic support. These results indicate that including UT/RT neuromuscular response in the haptic controller tuning procedure indeed improves overall user acceptance.

Over-tuning increases workload even over no haptic feedback

The results of the three subjective questionnaires indicate that acceptance of haptic cues increased for UT and RT haptic controllers, supporting the third hypothesis. The reduction of overall NASA TLX workload for UT/RT compared to NHF can be traced back to a reduction of mental load and effort. This is in sharp contrast to earlier research where haptic cues contributed negatively towards mental load and effort [15]. Over-tuning the controller was found to be more detrimental than providing no haptic support at all. This supports the notion that incorrect tuning can adversely impact user acceptance of HSC systems, and our formal tuning method provides a non-heuristic approach that prevents such incorrect tuning.

The optimal tuning range is relatively broad

For most dependent variables, no statistical differences were found between the admittance characteristics of the under- and relax-task tuned controllers; but both led to improved user acceptance relative to manual control.

The design space available for selecting an appropriate tuning profile is broader than expected and if either one should be preferred remains an open questions. Selection between the two tunings might be task specific. For tasks where the operator should be actively involved, e.g., in car driving [5], under-tuning the haptic controller (up to half the strength of the relax task controller) might provide a preferred option, since the operator needs to *actively agree* and comply with the guidance to correctly follow a prescribed trajectory (withing a range of acceptable trajectories). However, if failing to follow the haptic guidance might lead to an accident, as with collision avoidance systems, relax task tuning presents a better alternative. Such tuning ensures a successful collision avoidance, unless the operator, by stiffening up, *actively disagrees*.

Safety and performance alone are poor tuning metrics

As formulated in the first hypothesis the number of collisions was lower for stronger tuning profile (TP). The observed decrease, Fig. 10a, however, was not found to be statistically significant. The sample size used in this study ($n = 12$) was higher than the minimal $n_{\text{min}} = 5$ for a sufficient statistical power $1 - \beta = 0.8$ estimated based on effects observed in some similar haptic collision avoidance experiments [14], [15]. However, total $n_{collisions}$ for all conditions and participants in this study was substantially lower than in those previous studies. Based on the observed effect sizes, a recommended sample size for a future study would be $n_{\text{min}} = 20$. The low $n_{collisions}$ might be partially attributed to putting a strong emphasis on avoiding collisions during the task instructions and to the addition of the twenty second collision penalty.

Based on the results, and in accordance with the second hypothesis, TP had no measurable effect on performance. This may be due to subjects adapting their control strategies to ensure that task instructions are followed with similar performance for all TPs. This also suggests, that it would difficult to select an appropriate tuning setting using safety and performance metrics alone, whereas different tuning profiles do result in other differences.

The NMS admittance identification stage can be shortened

In accordance with findings of a previous study [32], the measured admittance responses of all subjects over tested conditions, Fig. 5, were similar. Moreover, the influence of bias force magnitude and direction followed a similar trend for all participants. This suggests, that to obtain a sufficient set of representative admittance measurements, for instance in a future practical application, a lower number of subjects and tested conditions could be used. The individual differences in the identified NMS setting fit within the UT/RT range, suggesting that there might be only little to gain in perusing an operator-individualized NMS tuning.

Haptics is appreciated when no visual feedback is available

Due to the limited lateral camera field of view supplied during the experiment, subjects had a greater appreciation for lateral haptic cues. It is interesting to note, that haptic activity decreased in the lateral direction, while control activity was found to be higher. Also the haptic controller agreement results show that agreement between the teleoperator and the haptic controller, both in terms of magnitude and direction of haptic moments, was better in the lateral direction. Due to the feedback architecture of the system, greater lateral stick

motion combined with a decrease in lateral haptic activity implies that subjects were more willing to follow lateral haptic cues. This maybe due to insufficient lateral visual cues, forcing subjects to rely on lateral haptic moments: for obstacles with sharp turns (obstacles 1, 4, 5 and 6) or when visual cues from the camera were not in the direction of motion (obstacle 3).

In the longitudinal direction, however, differences between the provided haptic and visual cues apparently led to 'goal' related conflicts. These conflicts need to be addressed in the future to further improve user acceptance of HSC systems. Control activity was lower than in the lateral direction, which can be attributed to the continuous corrective lateral stick inputs required to meet the secondary objective of flying through the center of waypoints.

VI. Conclusion and recommendations

We experimentally verified the effectiveness of using a formal tuning method for haptic shared controllers, based on relax-task setting of the neuromuscular system. For the studied conditions, we conclude that: 1) tuning based on safety and performance metrics alone would be difficult and the neuromuscular knowledge should be included; 2) tuning based on the relax task NMS setting was appreciated by the operators, with both physical and mental workload reduced; 3) this tuning optimum is; however, not sharp and both the under-tuned and the relax-task-tuned systems behaved equally well in the tested conditions and thus the requirements for the identification procedure could be reduced; 4) haptic feedback is most effective in directions with limited visual feedback; 5) in contrast, haptic feedback provided in the forward direction, where the operator had a good view, was more often opposed by the operators. Ways to minimize these conflicts should be investigated in future research.

References

[1] P. G. Griffiths and R. B. Gillespie, "Sharing Control Between Humans and Automation Using Haptic Interface: primary and secondary task performance benefits," *Human Factors: The Journal of the Human Factors and Ergonomics Society*, vol. 47, no. 3, pp. 574–590, 2005.

[2] D. A. Abbink, M. Mulder, and E. R. Boer, "Haptic shared control: smoothly shifting control authority?" *Cognition, Technology & Work*, vol. 14, no. 1, pp. 19–28, 2012.

[3] G. Baxter, J. Rooksby, Y. Wang, and A. Khajeh-Hosseini, "The ironies of automation: still going strong at 30?" in *Proceedings of the 30th European Conference on Cognitive Ergonomics*, Edinburgh, 2012, pp. 65–71.

[4] M. Olivari, F. M. Nieuwenhuizen, H. H. Bülthoff, and L. Pollini, "Pilot Adaptation to Different Classes of Haptic Aids in Tracking Tasks," *Journal of Guidance, Control, and Dynamics*, vol. 37, no. 6, pp. 1741–1753, Nov. 2014.

[5] D. A. Abbink and M. Mulder, "Exploring the Dimensions of Haptic Feedback Support in Manual Control," *Journal of Computing and Information Science in Engineering*, vol. 9, no. 1, p. 011006, 2009.

[6] D. A. Abbink, M. Mulder, F. C. T. van der Helm, M. Mulder, and E. R. Boer, "Measuring Neuromuscular Control Dynamics During Car Following With Continuous Haptic Feedback," *IEEE Transactions on Systems, Man, and Cybernetics, Part B: Cybernetics*, vol. 41, no. 5, pp. 1239 –1249, Oct. 2011.

[7] J. Smisek, M. M. van Paassen, M. Mulder, and D. A. Abbink, "Neuromuscular analysis based tuning of haptic shared control assistance for UAV collision avoidance," in *World Haptics Conference*, 2013, pp. 389–394.

[8] E. Sunil, J. Smisek, M. M. van Paassen, and M. Mulder, "Validation of a tuning method for haptic shared control using neuromuscular system analysis," in *Systems, Man and Cybernetics (SMC), 2014 IEEE International Conference on*. IEEE, 2014, pp. 1499–1504.

[9] P. W. Merlin, *Crash Course: Lessons Learned from Accidents Involving Remotely Piloted and Autonomous Aircraft*, ser. NASA Aeronautics Book Series. National Aeronautics and Space Administration, 2013.

[10] A. Franchi, C. Secchi, M. Ryll, H. H. Bülthoff, and P. Giordano, "Shared Control: Balancing Autonomy and Human Assistance with a Group of Quadrotor UAVs," *IEEE Robotics & Automation Magazine*, vol. 19, no. 3, pp. 57–68, Sep. 2012.

[11] A. M. Brandt and M. B. Colton, "Haptic collision avoidance for a remotely operated quadrotor uav in indoor environments," in *IEEE International Conference on Systems Man and Cybernetics*, Istanbul, 2010, pp. 2724–2731.

[12] H. I. Son, J. Kim, L. Chuang, A. Franchi, P. Giordano, D. Lee, and H. H. Bülthoff, "An evaluation of haptic cues on the tele-operator's perceptual awareness of multiple UAVs' environments," in *IEEE World Haptics Conference*, Istanbul, 2011, pp. 149 –154.

[13] S. M. Alaimo, L. Pollini, M. Innocenti, J. P. Bresciani, and H. H. Bülthoff, "Experimental comparison of direct and indirect haptic aids in support of obstacle avoidance for remotely piloted vehicles," *Journal of Mechanics Engineering and Automation*, vol. 2, pp. 2159–5275, 2012.

[14] T. M. Lam, "Haptic interface for UAV Teleoperation," Ph.D. dissertation, Delft University of Technology, 2009.

[15] T. M. Lam, M. Mulder, and M. M. van Paassen, "Haptic Interface For UAV Collision Avoidance," *The International Journal of Aviation Psychology*, vol. 17, no. 2, pp. 167–195, 2007.

[16] T. M. Lam, H. W. Boschloo, M. Mulder, and M. M. van Paassen, "Artificial Force Field for Haptic Feedback in UAV Teleoperation," *IEEE Transactions on Systems, Man and Cybernetics, Part A: Systems and Humans*, vol. 39, no. 6, pp. 1316–1330, 2009.

[17] D. A. Abbink, D. Cleij, M. Mulder, and M. M. van Paassen, "The importance of including knowledge of neuromuscular behaviour in haptic shared control," in *Systems, Man, and Cybernetics (SMC), 2012 IEEE International Conference on*. IEEE, 2012, pp. 3350–3355.

[18] D. A. Abbink and M. Mulder, "Neuromuscular analysis as a guideline in designing shared control," *Advances in haptics*, vol. 109, pp. 499–516, 2010.

[19] E. Sunil, "Tuning of a haptic collision avaoidance system for UAV teleoperation: Preliminary Report," Faculty of Aerospace Engineering, TU Delft, Delft, Preliminary, Aug. 2013.

[20] D. A. Abbink, "Neuromuscular Analysis of Haptic Gas Pedal Feedback during Car Following," PhD, Delft University of Technology, Delft, 2006.

[21] E. De Vlugt, "Identification of Spinal Reflexes," Ph.D. dissertation, Delft University of Technology, Delft, 2004.

[22] W. Mugge, D. A. Abbink, A. C. Schouten, J. P. A. Dewald, and F. C. T. van der Helm, "A rigorous model of reflex function indicates that position and force feedback are flexibly tuned to position and force tasks," *Experimental Brain Research*, vol. 200, no. 3-4, pp. 325–340, Jan. 2010.

[23] M. D. Penna, M. M. Van Paassen, D. Abbi, M. Mulder, M. Mulder, and others, "Reducing steering wheel stiffness is beneficial in supporting evasive maneuvers," in *Systems Man and Cybernetics (SMC), 2010 IEEE International Conference on*. IEEE, 2010, pp. 1628–1635.

[24] T. Tsuji, P. G. Morasso, K. Goto, and K. Ito, "Human hand impedance characteristics during maintained posture," *Biological Cybernetics*, vol. 72, no. 6, pp. 475–485, 1995.

[25] W. Mugge, D. A. Abbink, and F. C. T. van der Helm, "Reduced power method: how to evoke low-bandwidth behaviour while estimating full-bandwidth dynamics," in *International Conference on Rehabilitation Robotics*, Noordwijk, 2007, pp. 575–581.

[26] A. Schouten, E. de Vlugt, and F. van der Helm, "Design of Perturbation Signals for the Estimation of Proprioceptive Reflexes," *IEEE Transactions on Biomedical Engineering*, vol. 55, no. 5, pp. 1612–1619, May 2008.

[27] J. S. Bendat and A. G. Piersol, *Random data: analysis and measurement procedures*, 2nd ed. New York: Wiley, 1986.

[28] F. C. T. van der Helm, A. C. Schouten, E. De Vlugt, and G. G. Brown, "Identification of intrinsic and reflexive components of human arm dynamics during postural control," *Journal of Neuroscience Methods*, vol. 119, no. 1, pp. 1–14, 2002.

[29] E. J. Perreault, R. F. Kirsch, and P. E. Crago, "Effects of voluntary force generation on the elastic components of endpoint stiffness," *Experimental Brain Research*, vol. 141, no. 3, pp. 312–323, 2001.

[30] J. Smisek, E. Sunil, M. M. V. Paassen, D. A. Abbink, and M. Mulder, "Human operator limb neuromuscular admittance identified on a spring-centered control interface," [Dataset], DOI: 10.4121/uuid:cb7ddb1c-0bda-4434-a0b6-e8a31a071ac7, TU Delft, 2016.

[31] B. H. Krogh, "A generalized potential field approach to obstacle avoidance control," Society of Manufactuing Engineers, Tech. Rep., 1984.
[32] J. Lasschuit, T. Lam, M. Mulder, M. M. van Paassen, and D. A. Abbink, "Measuring and Modeling Neuromuscular System Dynamics for Haptic Interface Design," in *AIAA Modeling and Simulation Technologies Conference*, Honolulu, 2008.
[33] S. G. Hart and L. E. Staveland, "Development of NASA-TLX (Task Load Index): Results of Empirical and Theoretical Research," *Human Mental Workload*, vol. 1, no. 3, pp. 139–183, 1988.
[34] E. Jeannot, C. Kelly, and D. Thompson, *The development of situation awareness measures in ATM systems*. Brussels: Eurocontrol, 2003.
[35] A. Field, *Discovering Statistics using IBM SPSS Statistics*. London: Sage, 2013.

Jan Smisek (S'14) received the M.Sc. degree (cum laude) in Systems and Control from the Czech Technical University in Prague, Czech Republic, in 2011. Currently, he is working towards the Ph.D. degree at the Delft University of Technology, the Netherlands. He is also a Robotics Engineer at the Telerobotics and Haptics lab, with the European Space Research and Technology Centre (ESTEC) of the European Space Agency (ESA), situated in Noordwijk, the Netherlands. His research interests include teleoperation and shared autonomy.

Emmanuel Sunil received the M.Sc. degree in Aerospace Engineering (cum laude) from TU Delft in 2014, for his work on a haptic interface for unmanned aircraft collision avoidance. During his M.Sc. program, he did an internship at the Max Planck Institute for Biological Cybernetics in Tubingen, Germany. He is currently working as Ph.D. student at the Control and Simulation section of the faculty of Aerospace Engineering, TU Delft. His research focuses on airspace design, airborne separation assurance and airspace capacity modeling.

David A. Abbink (M'12–SM'14) received the M.Sc. and Ph.D. degrees in mechanical engineering from the Delft University of Technology, Delft, The Netherlands, in 2002 and 2006, respectively. He is an Associate Professor with the Delft Haptics Laboratory, Delft University of Technology. His current research interests include neuromuscular behavior, driver support systems, and haptics. Dr. Abbink is an associate editor of the IEEE Transactions on Human-Machine System.

Marinus M. (René) van Paassen (M'08–SM'15) received the M.Sc. degree (cum laude) from the Delft University of Technology, Delft, The Netherlands, in 1988, and a Ph.D. in 1994, both on studies into the neuromuscular system of the pilot's arm. He is an associate professor in Aerospace Engineering at the Delft University of Technology, working on human machine interaction and aircraft simulation. His work on human-machine interaction ranges from studies of perceptual processes, haptics and haptic interfaces and human manual control to design of and interaction with complex cognitive systems. René is a senior member of IEEE and of AIAA, and an associate editor for IEEE Transactions on Human-Machine System.

Max Mulder received the M.Sc. and Ph.D. degrees (cum laude) in aerospace engineering from the Delft University of Technology, Delft, The Netherlands, in 1992 and 1999, respectively, with a focus on the cybernetics of tunnel-in-the-sky displays. He is currently a Full Professor and the Head of the Control and Simulation Division, Faculty of Aerospace Engineering, Delft University of Technology. His current research interests include cybernetics and its use in modeling human perception and performance, and cognitive systems engineering and its application in the design of "ecological" human–machine interfaces.